Theory of four-wave mixing for bound and leaky modes

I. Allayarov [1,*] M. A. Schmidt [2,3] and T. Weiss [1]

[1]*4th Physics Institute and Research Center SCoPE, University of Stuttgart, Pfaffenwaldring 57, D-70550 Stuttgart, Germany*

[2]*Leibniz Institute of Photonic Technology, Albert-Einstein-Strasse 9, D-07745 Jena, Germany*

[3]*Otto Schott Institute of Material Research, Friedrich Schiller University Jena, Fraunhoferstrasse 6, D-07743 Jena, Germany*

(Received 10 January 2020; accepted 2 March 2020; published 7 April 2020)

We present a comprehensive theory of four-wave mixing in waveguide geometries, providing a rigorous description of the dynamics of both bound as well as leaky modes within a single theoretical framework. Our approach is based on the resonant-state expansion including analytical mode normalization. For bound modes, our approach agrees with the previous theory, while it results in modified nonlinear pulse propagation for leaky modes. For instance, it predicts a more efficient generation of Stokes and anti-Stokes bands with an earlier onset than expected from the previous theory for bound modes. These effects have been demonstrated numerically for a gas-filled hollow-core annulus fiber that supports leaky modes, rendering conventional bound-mode theory inappropriate for such systems. Moreover, we find that leaky modes provide modulation instability, not only in the anomalous but also in the normal dispersion regime. The modulation instability can occur for all frequencies, which is a fundamental difference to bound modes.

DOI: 10.1103/PhysRevA.101.043806

I. INTRODUCTION

One important nonlinear phenomenon that occurs in optical fibers due to the third-order nonlinear polarization is four-wave mixing [1], which has been studied extensively over the last several decades [2–7]. Traditionally, four-wave mixing is used to generate waves at certain frequencies or amplify a pre-existing weak signal [8,9]. At the same time, four-wave mixing is one of the main nonlinear mechanisms for supercontinuum generation in optical fibers in combination with self-phase and cross-phase modulations [1].

From the quantum physics point of view, the process of four-wave mixing relates to the annihilation of two incident (pump) photons at different frequencies and the simultaneous creation of two photons at new frequencies, while the laws of conservation of energy and momentum have to be fulfilled [see Fig. 1(a)]. Historically, the photons at new frequencies are either called Stokes (at lower frequency) or anti-Stokes (at higher frequency) photons. In this context, the process of annihilation of two photons at the same frequency is known as degenerate four-wave mixing. In optical fibers, four-wave mixing originates from the Kerr-type nonlinearity. Efficient four-wave mixing can only occur if there is no phase mismatch between pump, Stokes, and anti-Stokes waves. Therefore, observation and realization of four-wave mixing at desired frequencies requires dispersion-engineered waveguides with specific parameters.

Currently, hollow-core photonic crystal fibers represent a novel class of widely used fibers in the context of nonlinear photonics. They offer a plethora of additional degrees of freedom to control the optical properties compared to conventional fibers. For instance, the linear dispersion properties of gas-filled hollow-core fibers can be controlled through changing the gas temperature and the pressure, in addition to modifying its geometrical parameters, which, in fact, allows octave spanning supercontinua to be achieved [12,13]. On the other hand, geometric resonances of hollow-core fibers can be used for light generation [14]. Furthermore, using gases as a nonlinear medium allows for applying high-power laser sources without damaging the waveguide [15,16]. Additionally, nonlinear effects in such fibers can be enhanced by using liquids such as CS_2 or CCl_4 [17–20]. Within the context of this work, as a generic example of a hollow-core fiber geometry, we consider the annulus fiber geometry consisting of a single glass ring embedded in an otherwise low index medium [geometry depicted in Fig. 1(a)]. As shown in Ref. [21], this fiber geometry allows an accurate resemblance of the dispersion parameter of various kinds of hollow-core fibers and in particular, antiresonant fibers, making it a useful model system to study nonlinear pulse propagation in dissipative waveguide geometries.

Unlike conventional silica fibers that carry bound modes due to total internal reflection, hollow-core fibers support so-called leaky modes. As we can see from the example of the fundamental leaky mode of an annulus fiber [example in Fig. 1(b)], the electromagnetic fields of that mode grow with distance from the fiber center and transversely radiate with respect to the direction of propagation. Such a dissipative nature of the modes makes the application of standard theoretical formulations for the nonlinear pulse propagation in hollow-core fibers questionable, because the standard nonlinearity parameters are not defined uniquely for leaky modes due to the lack of rigorous mode normalization (e.g., the commonly used form of the normalization constant does not converge) [22–25]. Recently, we have solved the normalization issue by developing an analytical expression for the normalization, which can be readily applied to leaky

*i.allayarov@pi4.uni-stuttgart.de

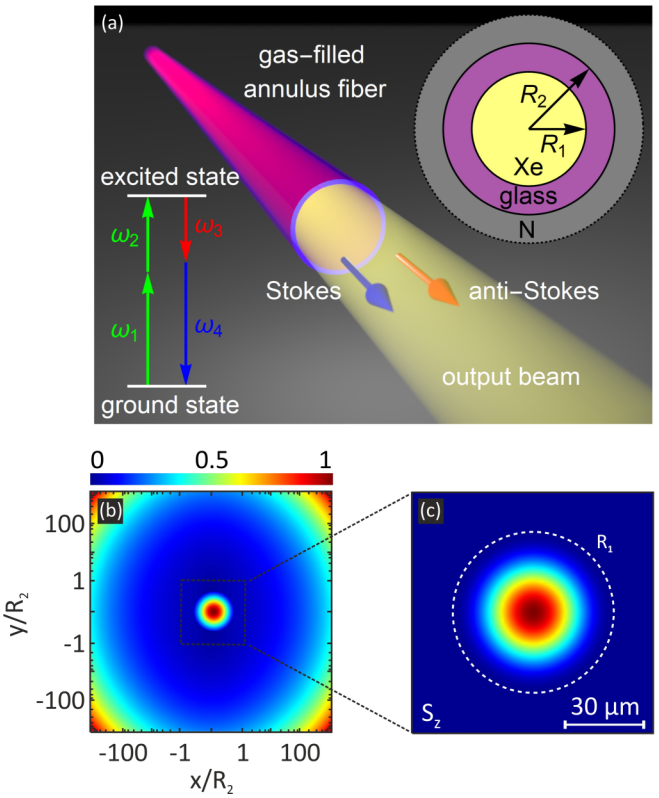

FIG. 1. (a) Cross section and schematics of an annulus fiber made from silica (SiO_2) and filled by xenon (Xe) in nitrogen (N) surrounding. The lower left inset shows energy-level diagram for four-wave mixing occurring due to the annihilation of two photons at frequencies ω_1 and ω_2 with creation of two new photons at frequencies ω_3 and ω_4. (b) Spatial distribution of the axial component of the real-valued Poynting vector of the fundamental leaky mode of the annulus waveguide geometry shown in (a). Outside the core region, a logarithmic scale is used for the distance to the fiber core. The white dashed line in (c) indicates the inner radius of the fiber. The refractive indices of silica and gases are taken from Refs. [10,11]. The inner and outer radii of the annulus waveguide are $R_1 = 30$ μm and $R_2 = 30.476$ μm, respectively (wavelength $\lambda = 470$ nm).

waveguide modes [26]. By combining the so-called resonant-state expansion [27–30] with this normalization scheme, we have derived a general master equation for the nonlinear pulse propagation inside optical fibers that is capable of treating both bound as well as leaky modes [31]. Here, we would like to emphasize that our approach is fully vectorial and follows *ab initio* from Maxwell's equations and does not require any slowly varying amplitude approximation. In the limit of single-mode propagation, our master equation transforms into the well-known standard nonlinear Schrödinger equation with a more general and accurate definition of the Kerr nonlinearity parameter. Interestingly, in the case of leaky modes, the Kerr nonlinearity parameter can either have a positive imaginary part corresponding to nonlinear loss [32–34] or exhibit a negative imaginary part that acts as nonlinear gain for overall attenuating fields. We have shown that the latter can have a significant impact on supercontinuum generation [31].

Here, we extend our theory for the nonlinear pulse propagation to four-wave mixing, requiring consideration of the coupling of excitations of several frequencies inside a single fiber. Owing to our mode normalization, the theory of four-wave mixing can be straightforwardly applied to complex waveguide geometries, including different types of hollow-core fibers. Most importantly, our theory allows for a rigorous description of not only bound modes but also leaky modes, in contrast to the scalar theory reported in literature [1]. Note that, in principle, one can extend the vectorial formulation developed in Ref. [35] to four-wave mixing and obtain similar coupled equations as in [1]. However, this approach is valid only for bound modes due to the absence of a rigorous normalization. We will consider this vectorial formulation, hereinafter referred to as bound-mode theory, as a reference for our theory of four-wave mixing.

Similar to the complex nonlinearity parameter with a negative imaginary part acting as nonlinear gain, we find that our four-wave mixing theory yields a regime with nonlinear gain and linear loss for leaky modes. In contrast to bound modes, our theory reveals that modulation instability can occur for leaky modes independently of the sign of the group velocity dispersion in the case of nonlinear gain. This means that small perturbations (e.g., given by phase noise) can be amplified even in the normal dispersion regime.

The paper is organized as follows: In Sec. II, we derive the coupled amplitude equations for four-wave mixing starting from our general master equation. Section III is devoted to the derivation of criterions for modulation instability. In Sec. IV, we provide details of our numerical simulations. Finally, we apply our theory to the example of a gas-filled annulus fiber and discuss the results in Sec. V.

II. COUPLED AMPLITUDE EQUATIONS

In order to derive the general form of coupled nonlinear propagation equations (in Gaussian units) for four-wave mixing in optical waveguides, let us first consider the transformation of the electric field $\mathbf{E}(\mathbf{r};t)$ to the frequency domain as

$$\mathbf{E}(\mathbf{r};\omega) = \int_{-\infty}^{+\infty} \mathbf{E}(\mathbf{r};t)e^{i\omega t}dt. \tag{1}$$

Next, we decompose $\mathbf{E}(\mathbf{r};\omega)$ into the fiber modes $\mathbf{E}_m(\mathbf{r}_{||};\omega)$ as

$$\mathbf{E}(\mathbf{r};\omega) = \sum_m a_m(z;\omega)\frac{\mathbf{E}_m(\mathbf{r}_{||};\omega)}{N_m(\omega)}, \tag{2}$$

where $a_m(z;\omega)$ is the modal amplitude (z is the axial direction), and $\mathbf{r}_{||}$ denotes the transverse coordinate in the xy plane [22]. The field distributions $\mathbf{E}_m(\mathbf{r}_{||};\omega)$ are eigensolutions of Maxwell's equations in the linear regime that can propagate with a phase factor $\exp[i\beta_m(\omega)z]$ along the fiber axis. Their normalization coefficient $N_m(\omega)$ has been derived in Ref. [26] and can be split into a line and a surface term:

$$N_m = L_m + S_m. \tag{3}$$

The line term yields

$$L_m = \frac{\varepsilon\mu k^2 + \beta_m^2}{2\left(\varepsilon\mu k^2 - \beta_m^2\right)^2}\int_0^{2\pi}\left(E_{m,z}\frac{\partial H_{m,z}}{\partial\phi} - H_{m,z}\frac{\partial E_{m,z}}{\partial\phi}\right)d\phi + \frac{k\beta_m\rho^2}{2\left(\varepsilon\mu k^2 - \beta_m^2\right)^2}\int_0^{2\pi}\left\{\mu\left[\left(\frac{\partial H_{m,z}}{\partial\rho}\right)^2 - \rho H_{m,z}\frac{\partial}{\partial\rho}\left(\frac{1}{\rho}\frac{\partial H_{m,z}}{\partial\rho}\right)\right] + \varepsilon\left[\left(\frac{\partial E_{m,z}}{\partial\rho}\right)^2 - \rho E_{m,z}\frac{\partial}{\partial\rho}\left(\frac{1}{\rho}\frac{\partial E_{m,z}}{\partial\rho}\right)\right]\right\}d\phi, \quad (4)$$

while the surface term is given by

$$S_m = \int_0^{2\pi}\int_0^{R}\rho(E_{m,\rho}H_{m,\phi} - E_{m,\phi}H_{m,\rho})d\rho d\phi. \quad (5)$$

Here, ε and μ are the permittivity and the permeability, respectively, and $k = \omega/c$ is the vacuum wave number. The electric and the magnetic fields of the mode, $\mathbf{E}_m(\mathbf{r};\omega)$ and $\mathbf{H}_m(\mathbf{r};\omega)$, respectively, are given in a cylindrical coordinate system, which is more convenient due to the cylindrical symmetry of the fiber geometry. Additionally, note that both the line term L_m and the surface term S_m are evaluated at a radius of normalization R that is typically finite, with the surface including all regions of spatial inhomogeneities in the transverse direction.

Based on these prerequisites, it has been shown that the evolution of the modal amplitude $a(z;\omega)$ can be described by the following general master equation [31]:

$$\partial_z a_m(z;\omega) = i\beta_m(\omega)a_m(z;\omega) + 2\pi ik\int \mathbf{e}_m^{\mathrm{R}}(\mathbf{r}_{||};\omega)\cdot\mathbf{P}_{\mathrm{NL}}(\mathbf{r}_{||},z;\omega)d\mathbf{r}_{||}, \quad (6)$$

where $\beta_m(\omega)$ is the frequency-dependent propagation constant, $\mathbf{e}_m^{\mathrm{R}}(\mathbf{r}_{||};\omega) \equiv \mathbf{E}_m^{\mathrm{R}}(\mathbf{r}_{||};\omega)/\sqrt{N_m(\omega)}$ is the normalized "reciprocal conjugate" transverse spatial distribution of the electric field of the fiber mode with propagation constant $-\beta_m(\omega)$, and ∂_z is the derivative along the z direction.

Several assumptions are introduced in the following to simplify Eq. (6). First, we restrict the analysis to the fundamental leaky core mode, which allows us to omit the mode index m in Eq. (6). Furthermore, the electric field $\mathbf{E}(\mathbf{r};\omega)$ is solely approximated by the electric field of the fundamental mode:

$$\mathbf{E}(\mathbf{r};\omega) \approx a(z;\omega)\,\mathbf{e}(\mathbf{r}_{||};\omega). \quad (7)$$

Next, we assume that optical pulses propagating in a fiber are narrow band and centered around carrier frequencies ω_j ($j = 1, 2, 3, \dots$). Thus, the electric field $\mathbf{E}(\mathbf{r};\omega)$ can be approximated as a superposition of the electric fields at these dominant carrier frequencies:

$$\mathbf{E}(\mathbf{r};\omega) \approx \sum_j a_j(z;\omega)\,\mathbf{e}(\mathbf{r}_{||};\omega_j). \quad (8)$$

Note that in Eq. (8) and following, the frequency dependence of the transverse spatial distribution of the electric field is assumed to be negligible (i.e., all fields are the same), i.e., $\mathbf{e}(\mathbf{r}_{||};\omega) \approx \mathbf{e}(\mathbf{r}_{||};\omega_j)$, and $a_j(z;\omega)$ is spectrally separated for the different dominant frequencies.

Furthermore, we make the typical approximation by expanding $\beta(\omega)$ into a Taylor series around ω_j:

$$\beta(\omega) \equiv \bar{\beta}(\omega) + i\bar{\alpha}(\omega) \approx \sum_{n\geqslant 0}\left(\frac{\bar{\beta}_j^{(n)}}{n!} + i\frac{\bar{\alpha}_j^{(n)}}{n!}\right)(\omega-\omega_j)^n, \quad (9)$$

where $\bar{\beta}_j^{(n)} = \partial^n\bar{\beta}/\partial\omega^n|_{\omega_j}$ and $\bar{\alpha}_j^{(n)} = \partial^n\bar{\alpha}/\partial\omega^n|_{\omega_j}$ are the nth-order dispersion and loss coefficients, respectively.

Additionally, we use that for narrow-band pulses with a carrier frequency ω_j, the modal amplitude $a_j(z;\omega)$ can be represented as

$$a_j(z;\omega) \equiv A_j(z;\Delta\omega)\,e^{i\bar{\beta}_j^{(0)}z}, \quad (10)$$

where $\Delta\omega \equiv \omega - \omega_j$. Thus, taking into account Eqs. (9) and (10), we obtain the following equation for $A_j(z;\Delta\omega)$:

$$\partial_z A_j(z;\Delta\omega) = \hat{D}_j(\Delta\omega)A_j(z;\Delta\omega) - 2\pi ik\,e^{-i\bar{\beta}_j^{(0)}z}\int\mathbf{e}^{\mathrm{R}}(\mathbf{r}_{||};\omega)\cdot\mathbf{P}_{\mathrm{NL}}(\mathbf{r}_{||},z;\omega)d\mathbf{r}_{||}, \quad (11)$$

where the dispersion operator $\hat{D}_j(\Delta\omega)$ is defined as

$$\hat{D}_j(\Delta\omega) = \sum_{n\geqslant 0}\left[i\frac{\bar{\beta}_j^{(n+1)}}{(n+1)!}\Delta\omega^{n+1} - \frac{\bar{\alpha}_j^{(n)}}{n!}\Delta\omega^n\right]. \quad (12)$$

Let us now address the nonlinear part of Eq. (11). As before, we assume that $\mathbf{e}^{\mathrm{R}}(\mathbf{r}_{||};\omega) \approx \mathbf{e}^{\mathrm{R}}(\mathbf{r}_{||};\omega_j) \equiv \mathbf{e}_j^{\mathrm{R}}(\mathbf{r}_{||})$, which allows us to avoid convolutions when transforming to the time domain. Furthermore, as in the case of the linear part of Eq. (11), we consider only the dominant frequencies. Thus, by carrying out the Fourier transform of Eq. (11) according to

$$A_j(z;t) = \frac{1}{2\pi}\int_{-\infty}^{+\infty}A_j(z;\omega-\omega_j)e^{-i(\omega-\omega_j)t}d\omega, \quad (13)$$

we obtain

$$\partial_z A_j(z;t) = \hat{D}_j(i\partial_t)A_j(z;t) - 2\pi ik_j\,e^{i\omega_j t - i\bar{\beta}_j^{(0)}z} \times\left(1 - \frac{1}{i\omega_j}\partial_t\right)\int\mathbf{e}_j^{\mathrm{R}}(\mathbf{r}_{||})\cdot\mathbf{P}_{\mathrm{NL}}(\mathbf{r};t)d\mathbf{r}_{||}. \quad (14)$$

Now, we have to specify the expression under the integral of Eq. (14). In general, the nonlinear polarization $\mathbf{P}_{\mathrm{NL}}$ can be expressed as a power series in the electric field $\mathbf{E} \equiv \mathbf{E}(\mathbf{r};t)$ as

$$\mathbf{P}_{\mathrm{NL}} = \chi^{(2)}(t) * \mathbf{EE} + \chi^{(3)}(t) * \mathbf{EEE} + \cdots, \quad (15)$$

where $\chi^{(n)}$ is the nth-order susceptibility, and $*$ denotes convolution in the time domain. In Eq. (15), the first term vanishes in most cases, since the second-order susceptibility $\chi^{(2)}$ equals zero for an isotropic medium such as liquids,

gases, and glasses [36]. Hence, we solely consider the third-order nonlinear term with $\chi^{(3)}$ as the dominating contribution in $\mathbf{P}_{\mathrm{NL}}$. While the higher-order contributions can become relevant in specific nonlinear polymers [e.g., polydiacetylene para-toluene sulfonate (PTS) [37]] and semiconductor-doped glasses at relatively high pulse intensity [38,39], their impact can be neglected in our case.

For relatively long pulses (>1 ps), which are considered here, we can furthermore neglect the contributions of molecular vibrations (Raman effect) to $\chi^{(3)}$ [40–43]. This allows us to consider an instantaneous nonlinear response, which is denoted as [1]

$$\mathbf{P}_{\mathrm{NL}} \approx \chi^{(3)}\vdots\mathbf{EEE}. \tag{16}$$

In general, due to the vectorial nature of the fields, $\chi^{(3)}$ is a fourth-rank tensor. The spatial symmetry of an isotropic medium restricts the form of $\chi^{(3)}$ to 21 nonzero elements, of which only two are independent. Additionally, by using intrinsic permutation symmetry of $\chi^{(3)}$ and taking into account the nonresonant electronic nature of the nonlinearity, the resulting nonlinear polarization becomes [36]

$$\mathbf{P}_{\mathrm{NL}} = \frac{\chi^{(3)}_{xxxx}}{4}[2\mathbf{E}(\mathbf{E}\cdot\mathbf{E}^*) + \mathbf{E}^*(\mathbf{E}\cdot\mathbf{E})]. \tag{17}$$

Since four-wave mixing involves the interaction between four waves at different frequencies ω_j ($j = 1-4$), the total electric field $\mathbf{E}(\mathbf{r};t)$ can be written as

$$\mathbf{E}(\mathbf{r};t) \approx \sum_{j=1}^{4} A_j(z;t)\,\mathbf{e}_j(\mathbf{r}_{||})\,e^{i\bar{\beta}_j^{(0)}z - i\omega_j t} + \mathrm{c.c.} \tag{18}$$

Taking into account Eqs. (17) and (18), the integral in Eq. (14) with prefactor $2\pi i k_j$ yields

$$\begin{aligned}
\mathrm{I}_{jlpq} &\equiv 2\pi i k_j \int \mathbf{e}_j^{\mathrm{R}}(\mathbf{r}_{||})\cdot\mathbf{P}_{\mathrm{NL}}(\mathbf{r}_{||},z;t)e^{i\omega_j t - i\bar{\beta}_j^{(0)}z}d\mathbf{r}_{||} \\
&= \underbrace{i\bar{n}_2 k_j \sum_{l,p,q}\int \left(\mathbf{e}_j^{\mathrm{R}}\cdot\mathbf{e}_l^*\right)(\mathbf{e}_p\cdot\mathbf{e}_q)A_l^*A_pA_q e^{i\phi_{pq,lj}}d\mathbf{r}_{||}}_{\equiv \mathrm{I}^{(1)}_{jlpq}} \\
&\quad + \underbrace{i\bar{n}_2 k_j \sum_{l,p,q}\int 2\left(\mathbf{e}_j^{\mathrm{R}}\cdot\mathbf{e}_l\right)(\mathbf{e}_p\cdot\mathbf{e}_q^*)A_lA_pA_q^* e^{i\phi_{lp,qj}}d\mathbf{r}_{||}}_{\equiv \mathrm{I}^{(2)}_{jlpq}},
\end{aligned} \tag{19}$$

where $\bar{n}_2 = 2\pi\chi^{(3)}_{xxxx}/4$ is the nonlinear refractive index, and the general phase difference $\phi_{jl,pq}$ is defined as

$$\begin{aligned}
\phi_{jl,pq} &= \Delta\bar{\beta}^{(0)}_{jl,pq}z - \Delta\omega_{jl,pq}t = \left[\left(\bar{\beta}_j^{(0)} + \bar{\beta}_l^{(0)}\right) - \left(\bar{\beta}_p^{(0)} + \bar{\beta}_q^{(0)}\right)\right]z \\
&\quad - [(\omega_j + \omega_l) - (\omega_p + \omega_q)]t.
\end{aligned} \tag{20}$$

The complete expression for Eq. (19) includes a large number of terms involving the products of three amplitudes. Nevertheless, we can distinguish the terms responsible for self-phase modulation, cross-phase modulation, and four-wave mixing. For instance, in the case that $q = p = l = j$, we obtain the following term for self-phase modulation:

$$\begin{aligned}
\mathrm{I}_{\mathrm{SPM}} &= i\left[\bar{n}_2 k_j \int \left[2\left(\mathbf{e}_j^{\mathrm{R}}\cdot\mathbf{e}_j\right)|\mathbf{e}_j|^2 + \left(\mathbf{e}_j^{\mathrm{R}}\cdot\mathbf{e}_j^*\right)\mathbf{e}_j^2\right]d\mathbf{r}_{||}\right]|A_j|^2A_j \\
&\equiv i\gamma_j|A_j|^2A_j,
\end{aligned} \tag{21}$$

with γ_j being the Kerr nonlinearity parameter [31]. Similarly, the sum over the index pairs ($p = j, q = l$), ($p = l, q = j$), and ($p = q = l, l = j$) provides terms for cross-phase modulation:

$$\begin{aligned}
\mathrm{I}_{\mathrm{XPM}} &= \mathrm{I}_{jljl} + \mathrm{I}^{(1)}_{jllj} + \mathrm{I}^{(2)}_{jjll} \\
&= i\Bigg[2\bar{n}_2 k_j \sum_{l\neq j}\int \left[\left(\mathbf{e}_j^{\mathrm{R}}\cdot\mathbf{e}_l\right)(\mathbf{e}_j\cdot\mathbf{e}_l^*) + \left(\mathbf{e}_j^{\mathrm{R}}\cdot\mathbf{e}_l^*\right)(\mathbf{e}_j\cdot\mathbf{e}_l)\right. \\
&\quad \left. + \left(\mathbf{e}_j^{\mathrm{R}}\cdot\mathbf{e}_j\right)|\mathbf{e}_l|^2\right]d\mathbf{r}_{||}\Bigg]|A_l|^2A_j \equiv i\sum_{l\neq j}\gamma_{jl}|A_l|^2A_j.
\end{aligned} \tag{22}$$

By collecting the terms for which $q \neq p \neq l \neq j$, we obtain the four-wave mixing contribution to Eq. (19):

$$\begin{aligned}
\mathrm{I}_{\mathrm{FWM}} &= \mathrm{I}^{(1)}_{jlpq} + \mathrm{I}^{(1)}_{jlqp} + \mathrm{I}^{(2)}_{jlpq} + \mathrm{I}^{(2)}_{jplq} \\
&= i\Bigg[2\bar{n}_2 k_j \int \left[\left(\mathbf{e}_j^{\mathrm{R}}\cdot\mathbf{e}_q\right)(\mathbf{e}_p\cdot\mathbf{e}_l^*) + \left(\mathbf{e}_j^{\mathrm{R}}\cdot\mathbf{e}_p\right)(\mathbf{e}_q\cdot\mathbf{e}_l^*)\right. \\
&\quad \left. + \left(\mathbf{e}_j^{\mathrm{R}}\cdot\mathbf{e}_l^*\right)(\mathbf{e}_p\cdot\mathbf{e}_q)\right]d\mathbf{r}_{||}\Bigg]A_l^*A_pA_q e^{i\Delta\bar{\beta}^{(0)}_{pq,lj}z} \\
&= i\gamma_{jlpq}A_l^*A_pA_q e^{i\Delta\bar{\beta}^{(0)}_{pq,lj}z}.
\end{aligned} \tag{23}$$

In the particular case of $q \neq p \neq l = j$ (or $q = p \neq l \neq j$), Eq. (23) corresponds to degenerate four-wave mixing.

In general, Eq. (19) contains many other phase terms responsible for phenomena such as frequency tripling ($\omega_q = \omega_j + \omega_l + \omega_p$) or other frequency conversion processes (e.g., $\omega_q = 2\omega_j + \omega_p$). Here, we neglect such contributions, since from the quantum-mechanical point of view, the probability of these processes is rather low [1]. Additionally, we neglect the time derivative term on the right-hand side of Eq. (14) that accounts for the dispersion of the nonlinearity, leading to nonlinear effects such as self-steepening and optical shock formation, which become important only for femtosecond pulses [1]. Therefore, we keep only all dominant terms that are responsible for processes such as self-phase modulation, cross-phase modulation, and four-wave mixing. Under these assumptions, Eq. (14) applied to each field at frequencies ω_j ($j = 1-4$) leads to the following set of four coupled amplitude equations:

$$\partial_z A_1 = (\hat{D}_1 + \hat{N}_1)A_1 + i\gamma_{1234}A_2^*A_3A_4e^{i\Delta\bar{\beta}^{(0)}z}, \tag{24a}$$

$$\partial_z A_2 = (\hat{D}_2 + \hat{N}_2)A_2 + i\gamma_{2134}A_1^*A_3A_4e^{i\Delta\bar{\beta}^{(0)}z}, \tag{24b}$$

$$\partial_z A_3 = (\hat{D}_3 + \hat{N}_3)A_3 + i\gamma_{3412}A_4^*A_1A_2e^{-i\Delta\bar{\beta}^{(0)}z}, \tag{24c}$$

$$\partial_z A_4 = (\hat{D}_4 + \hat{N}_4)A_4 + i\gamma_{4312}A_3^*A_1A_2e^{-i\Delta\bar{\beta}^{(0)}z}, \tag{24d}$$

with the nonlinear operator

$$\hat{N}_j \equiv i\left(\gamma_j|A_j|^2 + \sum_{l\neq j}\gamma_{jl}|A_l|^2\right), \tag{25}$$

and the wave-vector mismatch between the input and output waves

$$\begin{aligned}\Delta\bar{\beta}^{(0)} &\equiv \Delta\bar{\beta}^{(0)}_{34,21} = \Delta\bar{\beta}^{(0)}_{34,12} = -\Delta\bar{\beta}^{(0)}_{12,43} = -\Delta\bar{\beta}^{(0)}_{12,34}\\ &= \bar{\beta}^{(0)}_3 + \bar{\beta}^{(0)}_4 - \bar{\beta}^{(0)}_1 - \bar{\beta}^{(0)}_2.\end{aligned} \tag{26}$$

This system of Eqs. (24a)–(24d) describes four-wave mixing for bound and leaky modes. As we can see, the contribution of the last coupling term (i.e., efficiency of four-wave mixing) becomes significant if this wave-vector mismatch vanishes, i.e., $\Delta\bar{\beta}^{(0)} = 0$.

It should be noted that a similar form of Eq. (19) can be also derived by using the standard theory of bound modes [1,35]. In that case, however, reciprocal conjugation would be replaced by complex conjugation. While reciprocal conjugation and complex conjugation of modes are identical operations for bound modes, they yield different results for leaky modes. Moreover, leaky modes require a correct normalization, which is provided by Eqs. (3)–(5). Therefore, all nonlinearity coefficients in Eqs. (24a)–(24d) deviate from those of the conventional bound-mode theory when considering leaky modes. Particularly, they exhibit a nonvanishing imaginary part that is either positive, corresponding to nonlinear loss [32–34], or negative acting as nonlinear gain for overall attenuating fields [31]. In the next sections, we numerically analyze the impact of our new formulation on four-wave mixing of leaky modes by comparing it with results that are based on applying the bound-mode theory to leaky modes. In order to do that, we basically ignore any issues with the normalization of bound modes using the conventional theory and assume that the real part of the nonlinearity coefficients has been calculated correctly, while we neglect its imaginary part.

As it has been mentioned at the beginning of this section, all equations in this work are given in Gaussian units, consistent with our previous works. However, one can straightforwardly reformulate the equations in SI units by using the following changes: The permittivity ε and permeability μ have to be replaced by the relative ones, and one needs to substitute $\mathbf{H}$ with $Z_0\mathbf{H}^{\mathrm{SI}}$, where Z_0 is the vacuum impedance, while $\mathbf{E}$ simply becomes $\mathbf{E}^{\mathrm{SI}}$. Next, for the conversion of the third-order susceptibility from Gaussian to SI units we can use $\chi^{(3)} = 4\pi/(3\times 10^4)^2\,[\chi^{(3)}]^{\mathrm{SI}}$ [44]. In order to allow for an easier comparison with experimental results, we present our simulation results in the following sections in SI units.

III. MODULATION INSTABILITY OF PULSES IN HOLLOW-CORE WAVEGUIDES

In general, the system of Eqs. (24a)–(24d) describes narrow-band pulses that are spectrally separated. However, for small frequency spacings (<1 THz), it is more convenient to use a single nonlinear Schrödinger equation with a certain initial condition [1]. In that case, an interaction between the nonlinear and dispersive effects can lead to the generation of new frequencies from noise, which is also known as modulation instability [1]. Typically, the nonlinearity parameter γ is assumed to be a real quantity in the stability analysis of the modulations. However, as mentioned in the Introduction, the nonlinearity parameter γ has a negative imaginary part for hollow-core fibers supporting leaky modes that can act as a nonlinear gain, partially diminishing the impact of modal attenuation during propagation [31]. Hence, we observe here an interplay between nonlinear gain and modal loss besides self-phase modulation and group velocity dispersion. In this section, we derive steady-state solutions in this regime and analyze their stability against small perturbations.

For the sake of simplicity, we consider the standard nonlinear Schrödinger equation with a complex nonlinearity parameter and linear loss:

$$i\partial_z A - \frac{\bar{\beta}^{(2)}}{2}\partial_\tau^2 A + (\gamma_r + i\gamma_i)|A|^2 A + i\bar{\alpha}A = 0. \tag{27}$$

Here, A is the field amplitude, $\bar{\beta}^{(2)}$ is the second-order dispersion coefficient, $\bar{\alpha}>0$ is the modal loss coefficient, and γ_r (>0 self-focusing, <0 self-defocusing) and γ_i (>0 nonlinear loss, <0 nonlinear gain) are the real and imaginary parts of the nonlinearity parameter γ, respectively. Below, we consider the self-focusing case. Additionally, we introduced the retarded time coordinate of $\tau = t - \bar{\beta}^{(1)}z$ along the propagation direction z.

Considering Eq. (27) as a dynamical system yields the following steady-state solution [45,46]:

$$A = A_0\, e^{i\gamma_r|A_0|^2 z}, \tag{28}$$

where $A_0 = \sqrt{-\bar{\alpha}/\gamma_i}$. This basically means that we require a suitable balance between linear attenuation and nonlinear gain.

In order to investigate modulation instability, we add a small perturbation to the steady-state solution [1]:

$$\tilde{A} = [A_0 + a(z,\tau)]\, e^{i\gamma_r|A_0|^2 z} = A + a\, e^{i\gamma_r|A_0|^2 z}, \tag{29}$$

where $a(z,\tau)$ is the small perturbation. Substituting Eq. (29) in Eq. (27) and linearizing $a(z,\tau)$, after some algebra we obtain the following:

$$i\partial_z a - \frac{\bar{\beta}^{(2)}}{2}\partial_\tau^2 a + (\gamma_r + i\gamma_i)|A_0|^2(a + a^*) = 0. \tag{30}$$

A general solution of Eq. (30) can be written as

$$a(z,\tau) = u(z)\, e^{i\Omega\tau} + v^*(z)\, e^{-i\Omega\tau}, \tag{31}$$

where $u(z)$ and $v(z)$ are the coefficients determined by solving Eq. (30), and Ω is the frequency of the modulation.

By introducing $b = u + v$ and $c = u - v$ and by inserting Eq. (31) into Eq. (30), we obtain the following system of homogeneous equations:

$$\partial_z\begin{bmatrix} b\\ c\end{bmatrix} = \underbrace{\begin{bmatrix} -2\gamma_i|A_0|^2 & i\frac{\bar{\beta}^{(2)}}{2}\Omega^2\\ i\frac{\bar{\beta}^{(2)}}{2}\Omega^2 + 2i\gamma_r|A_0|^2 & 0\end{bmatrix}}_{M}\begin{bmatrix} b\\ c\end{bmatrix}. \tag{32}$$

Searching for the eigenvalues Γ of the matrix M, we obtain a characteristic equation of the form

$$\Gamma^2 + 2\gamma_i|A_0|^2\Gamma + \frac{\bar{\beta}^{(2)}}{2}\Omega^2\left(\frac{\bar{\beta}^{(2)}}{2}\Omega^2 + 2\gamma_r|A_0|^2\right) = 0, \tag{33}$$

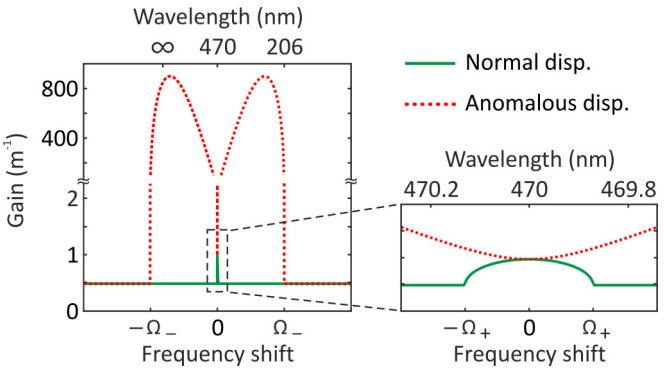

FIG. 2. Gain spectra of modulation instability at a pump wavelength of $\lambda = 470$ nm for the annulus fiber with $\gamma = (8.47 \times 10^{-6} - 4.58 \times 10^{-9} i)\ \mathrm{m^{-1}\,W^{-1}}$, $\alpha = 0.24\ \mathrm{m^{-1}}$, and $|\bar{\beta}^{(2)}| = 6.84 \times 10^{-2}\ \mathrm{ps^2\,km^{-1}}$. The red dashed line indicates the gain spectrum of modulation instability calculated in the anomalous dispersion regime with $\mathrm{sgn}(\bar{\beta}^{(2)}) = -1$, while the solid green line is obtained for $\mathrm{sgn}(\bar{\beta}^{(2)}) = 1$, corresponding to the normal dispersion regime. Note that in both cases, there is a nonzero gain for all frequencies.

which has the solutions

$$\Gamma_\pm = -\gamma_i |A_0|^2 \pm \sqrt{(\gamma_i |A_0|^2)^2 - \left(\frac{\bar{\beta}^{(2)}}{2}\Omega\right)^2 \left(\Omega^2 + \mathrm{sgn}(\bar{\beta}^{(2)})\,\Omega_c^2\right)}, \tag{34}$$

where $\mathrm{sgn}(\bar{\beta}^{(2)}) = \pm 1$, depending on the sign of $\bar{\beta}^{(2)}$ and $\Omega_c^2 = 4\gamma_r |A_0|^2/|\bar{\beta}^{(2)}|$. This yields $b(z) = b_+ \exp(\Gamma_+ z) + b_- \exp(\Gamma_- z)$ and $c(z) = c_+ \exp(\Gamma_+ z) + c_- \exp(\Gamma_- z)$, where $b_\pm$ and $c_\pm$ depend on the initial conditions for the perturbation a. Note that Γ can be related to a wave number K of the perturbation as $\Gamma = iK$. In fact, perturbations can grow exponentially along the fiber in the regime with $\gamma_i < 0$, since the first line on the right-hand side of Eq. (34) always yields a nonvanishing positive real part for any real Ω. Interestingly, this does not depend on the sign of $\bar{\beta}^{(2)}$—in contrast to the modulation instability described in the literature, which occurs only in the anomalous dispersion regime ($\bar{\beta}^{(2)} < 0$) at certain frequencies [1].

Furthermore, we also note that the first line on the right-hand side of Eq. (34) does not depend on frequency. This already indicates that the modulation instability can occur at any wavelength. For further analysis of the results, we introduce the gain spectrum defined as $g(\Omega) = 2\,\mathrm{Re}(\Gamma)$. As we can deduce from Eq. (34), the gain is minimal if the expression under the square root is negative. This minimal or "background" gain is given by $g_{\min} = -2\gamma_i |A_0|^2 = 2\alpha$ for frequencies Ω with

$$\Omega^2 \geqslant \Omega_\pm^2 \equiv \frac{1}{2}{\Omega_c}^2 \left[\sqrt{1 + \left(\frac{\gamma_i}{\gamma_r}\right)^2} \mp 1\right], \tag{35}$$

where Ω_+ and Ω_- correspond to the normal and the anomalous dispersion, respectively.

As we can see in Fig. 2, inside the frequency window $\Omega^2 < \Omega_\pm^2$, the gain spectrum can always exceed $g_{\min}$. It has two maxima at $\Omega = \pm\Omega_c/\sqrt{2}$ in the anomalous dispersion regime (red dashed line), while in the case of normal dispersion (green solid line) $g(\Omega)$ is maximum at $\Omega = 0$.

Here, we note that the steady-state solution of Eq. (27) and, accordingly, the dispersion relation Eq. (34), are determined uniquely by the fiber parameters. Waves with such properties are sometimes called autowaves [47]. Particularly, localized waves in gain-loss-balanced nonlinear systems are referred to as autosolitons or dissipative solitons [48]. Furthermore, similar systems have been investigated in different frameworks, such as the Benjamin-Feir instability of water waves [49], nonequilibrium pattern forming within the Ginzburg-Landau models [45], and vector modulation instability in birefringent fibers [50].

IV. FIBER AND SIMULATION DETAILS

Here, we provide geometrical and optical parameters of the fiber as well as details of the nonlinear pulse propagation. For our numerical simulations, we consider an annulus fiber made from silica (SiO_2) and filled by xenon (Xe) with a nitrogen (N) surrounding [see Fig. 1(a)]. The inner radius and thickness of the annulus are $R_1 = 30$ μm and $\Delta R = 0.476$ μm, respectively. The optical parameters of this waveguide, such as the linear and nonlinear refractive indices, are taken from Refs. [10,11,51,52]. Here, we assume that the pressure inside (Xe) and outside (N) the fiber are 1 and 4 bar, respectively. Thus, with these geometrical and optical parameters of the annulus fiber we are able to design a dispersion curve such that it yields a strong impact of our theory.

The modal properties of the fiber are found by solving Maxwell's equations. Following the procedures described in the literature [22,53], we can derive an eigenvalue equation for the propagation constant β. Panels (a) and (b) in Fig. 3 display the real and imaginary parts of the effective refractive index $n_{\mathrm{eff}} = \beta/k$ of the fundamental leaky mode of the fiber as a function of wavelength. Since the silica layer can be considered as a Fabry-Perot–type resonator, it has resonances at the wavelengths $\lambda = 2\Delta R/m\,[n_{\mathrm{SiO_2}}^2(\lambda) - n_{\mathrm{Xe}}^2(\lambda)]^{1/2}$, where $m = 1, 2, \ldots$ [54] with the modal loss [$\mathrm{Im}(n_{\mathrm{eff}})$] having its maxima at these resonances. In the wavelength range considered in Fig. 3, we can see the second ($m = 2$) resonance at $\lambda = 507$ nm.

Next, we use the solutions of the eigenvalue problem to calculate the nonlinear parameters. For instance, panels (c) and (d) in Fig. 3 display the real and imaginary parts of the nonlinearity parameter γ of the fundamental leaky mode of the fiber as a function of wavelength. In these panels, the red solid line indicates the results obtained by using the resonant-state expansion, while the blue dots are based on the results of bound-mode theory. Details about the difference between resonant-state expansion and bound-mode theory can be found at the end of Sec. II. We note that in both cases the contribution of the surrounding gas, i.e., nitrogen, to the nonlinear parameters is neglected, since $\chi^{(3)}_{\mathrm{SiO_2}} \gg \chi^{(3)}_{\mathrm{Xe}} \gg \chi^{(3)}_{\mathrm{N}}$ [52]. Furthermore, we can consider the smallest region with spatial inhomogeneities, i.e., $R = R_2$ as the radius of normalization in Eq. (3). In the case of bound-mode theory, fiber modes are usually normalized with respect to the axial

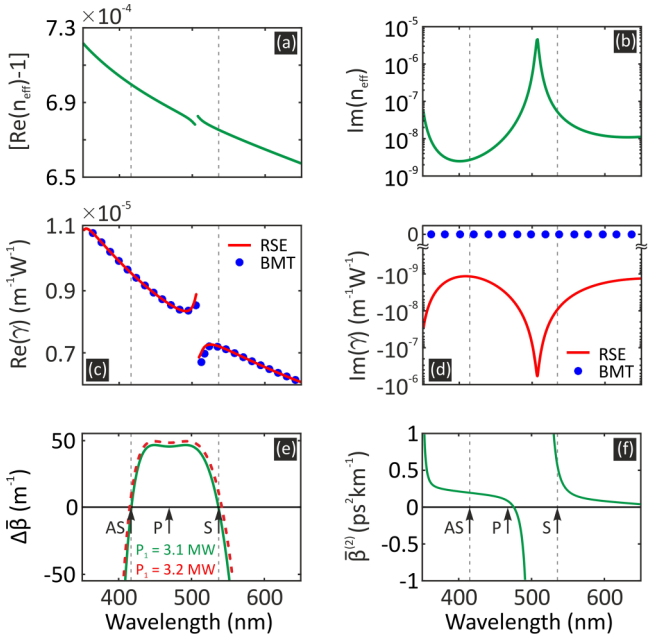

FIG. 3. Spectral distributions of the various relevant parameters. (a) Real and (b) imaginary parts of the effective refractive index for the fundamental leaky mode of the annulus fiber shown in Fig. 1(a). Comparisons of results obtained by the resonant-state expansion (RSE) and the bound-mode theory (BMT) are given in panels (c) and (d), respectively, for the real and imaginary parts of the nonlinearity parameter of that mode. (e) Phase mismatch for degenerate four-wave mixing at a pump wavelength of 470 nm and initial powers of 3.1 MW (green solid line) and 3.2 MW (red dashed line), respectively. The central arrow indicates the position of pump (P) wave, while the side arrows indicate the estimated positions of the Stokes (S) and the anti-Stokes (AS) bands that occur at the wavelength with vanishing phase mismatch. (f) Second-order dispersion coefficient. All three waves are in the normal dispersion region. The gray vertical dashed lines in all panels indicate the spectral positions of the Stokes and the anti-Stokes waves.

component of the time-averaged Poynting vector with a radius of normalization of $R = \infty$. However, an infinite radius of normalization applied to leaky modes yields a vanishing value for the nonlinearity parameter γ, since the fields of leaky modes diverge [see Fig. 1(b)]. Therefore, we choose the radius of normalization such that the deviation of the real part of γ between the resonant-state expansion and the bound-mode theory is minimized. As we can see in Fig. 3(c), the real part of the nonlinearity parameter γ is similar in both approaches. However, the bound-mode theory solely provides a purely real γ.

The estimated positions of the Stokes and anti-Stokes waves for particular pump wave parameters (wavelength and power) are defined by the phase-matching condition. In order to have the most efficient side-band generation, it is necessary to compensate the linear wave-vector mismatch $\Delta\bar{\beta}^{(0)}$ between the pump and side bands with the nonlinear phase shifts caused by self-phase and cross-phase modulations. For the sake of simplicity we consider degenerate four-wave mixing, for which $\omega_1 = \omega_2$. In this case, we can write the phase-matching condition as follows [1]:

$$\Delta\bar{\beta} = \left[\bar{\beta}^{(2)}\Omega_s^2 + \frac{\bar{\beta}^{(4)}}{12}\Omega_s^4\right] + 2\gamma_r P_1 \approx 0. \tag{36}$$

Here, $\Omega_s = \omega_1 - \omega_3 = \omega_4 - \omega_1$ is the frequency shift with respect to the pump frequency ω_1, $\bar{\beta}^{(2)}$ and $\bar{\beta}^{(4)}$ are the dispersion parameters at ω_1, and γ_r is the real part of the nonlinearity parameter γ at the pump frequency.

In order to exclude a strong impact of modulation instability and consider rather typical four-wave mixing, we choose the pump wave parameters such that all (i.e., the pump and Stokes) waves are in the normal dispersion regime. In this case, the phase-matching condition can be satisfied if $\bar{\beta}^{(4)} < 0$. For example, as shown in Fig. 3(d), for the pump wave with an initial power of $P_1 = 3.1$ MW and a wavelength of $\lambda_1 = 470$ nm, at which $\bar{\beta}^{(2)} = 6.84 \times 10^{-2}$ ps^2 km^{-1}, $\bar{\beta}^{(4)} = -1.14 \times 10^{-5}$ ps^4 km^{-1}, and $\gamma_r = 8.47 \times 10^{-6}$ m^{-1} W^{-1}, the phase mismatch vanishes at wavelengths of $\lambda_3 = 540.6$ nm (Stokes) and $\lambda_4 = 415.8$ nm (anti-Stokes). In Fig. 3(e), we see that all three (i.e., the pump, Stokes, and anti-Stokes) waves are in the normal dispersion region. The positions of the side bands can be easily tuned by varying the pump wave parameters.

So far, we have drawn our attention to determine the parameters of the fiber that enter Eqs. (24a)–(24d), while in the following we discuss the details of the numerical simulations. As an initial condition for the amplitude of the pump pulse, we consider a hyperbolic secant profile $A_1(0,t) = \sqrt{P_1}\,\mathrm{sech}(t/T_0)$ with the initial width $T_0 = 100$ ps. For such a relatively long pulse, we can neglect higher-order dispersion and loss terms, and nonlinear effects such as self-steepening and Raman scattering [1]. Hence, the real and imaginary parts of the propagation constant $\beta(\omega) = \bar{\beta}(\omega) + i\bar{\alpha}(\omega)$ are approximated by corresponding Taylor series expansions up to $\bar{\beta}^{(4)}$ and $\bar{\alpha}^{(2)}$ as the fourth and second order, respectively. Furthermore, we assume that the pump, Stokes, and anti-Stokes wavelengths have the same group velocities $v_g \equiv 1/\bar{\beta}^{(1)}$, since the relative difference of v_g between them is negligible, i.e., is less than $\Delta v_g/v_g < 10^{-5}$. The initial amplitudes for the Stokes A_3 and anti-Stokes A_4 waves are given by $A_{3,4}(0,t) = \sqrt{P_{3,4}}\,\mathrm{sech}(t/T_0)\exp(\mp i\Omega_s t)$, where $P_{3,4} \ll P_1$ and the "-" sign is for A_3. We choose $P_{3,4}$ such that a seed for the Stokes and anti-Stokes waves at the corresponding frequencies is at the level of the spectral background (noise) of the pump field [55].

The numerical solution of Eqs. (24a)–(24d) is carried out by using an improved version of the well-known split-step-Fourier method [1]. Here, the linear part of the equations is solved in the frequency domain, while for the nonlinear part, a fourth-order Runge-Kutta method is used [56,57]. In our numerical simulations, we use $N = 2^{22}$ points to discretize a time window of $T_{\mathrm{Span}} = 100\,T_{\mathrm{FWHM}}$. These parameters provide a wavelength window of $\lambda_{\mathrm{Span}} = cN/T_{\mathrm{Span}} \sim 320$–$770$ nm, according to the sampling theorem, which entirely covers the spectral range of our interest. The longitudinal step size used in numerical simulations is $\Delta z = 40\,\mu$m.

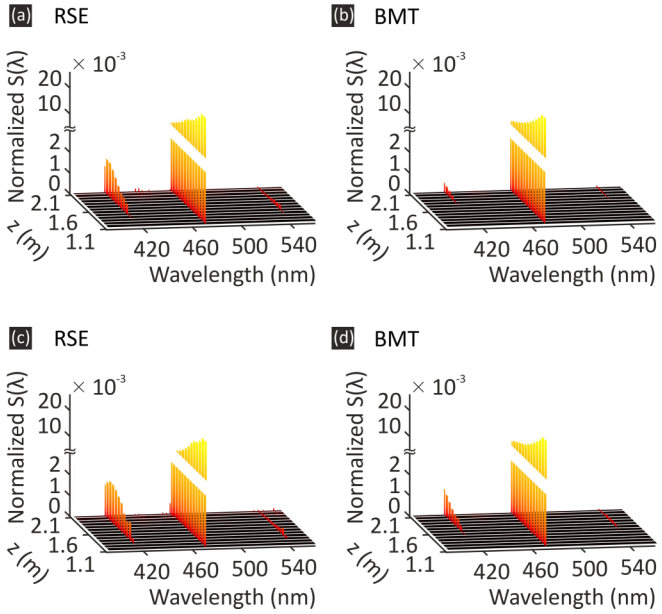

FIG. 4. Spatial-spectral evolution of the total power-spectral-density $S(\lambda)$ obtained by using our theory based on the resonant-state expansion and the bound-mode theory for an initial pump power of 3.1 MW [panels (a) and (b)] and 3.2 MW [panels (c) and (d)], respectively. Note that the total power spectral density $S(\lambda)$ is normalized to the initial power density. All other simulation parameters can be found in Ref. [55].

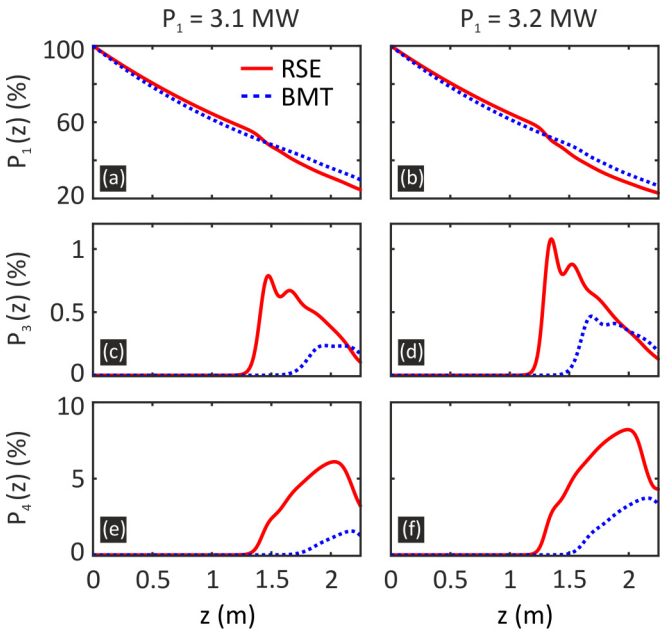

FIG. 5. Normalized pump [panels (a) and (b)], Stokes [panels (c) and (d)], and anti-Stokes [panels (e) and (f)] power as a function of propagation distance. The results have been obtained by using our theory based on the resonant-state expansion (red solid line) and the bound-mode theory (blue dashed line) for initial pump powers of 3.1 MW (left column) and 3.2 MW (right column).

V. RESULTS AND DISCUSSION

The analysis of the pulse dynamics starts by investigating the total power spectral density $S(\lambda)$, which is normalized to the initial power density. Panel (a) in Fig. 4 depicts $S(\lambda)$ dynamics based on our formulation for the initial pump power of $P_1 = 3.1$ MW, while the results in panel (b) are based on the bound-mode theory. Note that the final equations become similar for both cases. The main difference is in the definition of the nonlinearity parameters. In the first case, the nonlinearity parameter γ has a negative imaginary part in contrast to the latter [see Fig. 3(d)]. In addition, reciprocal conjugation is replaced by complex conjugation in the bound-mode theory. More details about the difference between two models can be found at the end of Sec. II. By comparing panels (a) and (b) of Fig. 4, we clearly see that our formulation yields more pronounced side bands. This is a substantial effect, considering that $\mathrm{Im}(\gamma)/\mathrm{Re}(\gamma)$ is rather small. Due to the higher modal loss at the Stokes position ($\lambda_3 = 540.6$ nm) compared to the anti-Stokes one ($\lambda_4 = 415.8$ nm), the power spectral density of the Stokes wave is comparably low [see Fig. 3(b)]. Please note that we use a broken power axis to show the side bands clearly.

Let us now repeat our simulations for a higher initial pump power of $P_1 = 3.2$ MW for the same pump wavelength. In this case, the positions of the side bands are slightly shifted according to the phase-matching condition [see Fig. 3(e)]. However, they are still in the normal dispersion regime, and all other parameters are close to those of the previous case. As we can see in panels (c) and (d) of Fig. 4, the Stokes and anti-Stokes bands are generated with a higher power spectral density. Specifically, the gain is larger in the bound-mode theory [compare panels (b) and (d)] than in our formulation based on the resonant-state expansion [compare panels (a) and (c)]. The reason for the latter is that the impact of the nonlinear gain contribution [i.e., terms proportional to $\mathrm{Im}(\gamma)|A_1|^2$] to the side-band generation is decreasing due to the strong pump power ($P_1 \propto |A_1|^2$) depletion when using the resonant-state expansion. Moreover, the spectral broadening of the pump and side bands and their interaction generates various new frequencies, giving rise to supercontinuum generation at larger propagation distances. Therefore, in Fig. 4 we have truncated the nonlinear pulse dynamics at around $z = 2.1$ m.

Now, let us consider the efficiency of the side-band generation. For that, we calculate the total power of each wave by integrating the corresponding total power spectral density $S(\lambda)$ over wavelength for each step of propagation. In Fig. 5, we plot the total power of the pump (P_1), Stokes (P_3), and anti-Stokes (P_4) waves normalized to the initial total power of the pump wave as a function of propagation distance z. The red solid lines indicate the power calculated by using our formulation, while the blue dashed lines express the results based on the bound-mode theory. In the left column [panels (a), (c), and (e)], we display the results for the initial pump power of $P_1 = 3.1$ MW. First, we clearly recognize that in our formulation, the Stokes and anti-Stokes bands exhibit at least two times more maximum power. Second, the most interesting point is that in our case, the Stokes and anti-Stokes bands occur roughly 50 cm earlier than in the bound-mode theory. An efficient power transfer from the pump to the side bands is observed at around $z = 1.5$ m, where the pump power sharply starts to decrease. Furthermore, we can see an oscillatory

behavior of their total power over distance, which is clearly pronounced in the case of the Stokes band and relates an exchange of power between the two excitations.

The situation for the initial pump power of $P_1 = 3.2$ MW (the right column) is very similar to the previous case. As a main difference, we note the following: Increasing the initial pump power leads to generation of Stokes and anti-Stokes bands with higher power within the phase-matching condition. Additionally, the onset of the side-band generation arises earlier in both bound-mode theory and resonant-state expansion. Compared to $P_1 = 3.1$ MW, the onset is roughly 20 cm earlier. Common to both initial pump powers is that the side bands decay at long distances, which might be due to the pump depletion and modal losses.

VI. SUMMARY

In conclusion, we have presented here a general theoretical formulation for a rigorous description of four-wave mixing in waveguide geometries. The formulation is based on the so-called resonant-state expansion with analytic mode normalization, which allows consideration of both bound and leaky modes within a single framework. For a proof-of-concept analysis and as an example system, we have applied our theory to a gas-filled hollow-core annulus fiber. The numerical results reveal that our formulation predicts a more efficient generation of the Stokes and anti-Stokes bands with an earlier onset for the leaky mode system in comparison with the bound-mode theory. Our findings originate from an accurate description of the nonlinear properties and, in particular, of the nonlinearity parameter of the considered waveguide.

While we do not have any experimental results yet, the comparison of bound-mode theory and our theory reveals that the conventional bound-mode theory is inappropriate for capturing all phenomena that arise during the propagation of leaky modes. Therefore, we believe that our theory for four-wave mixing can help to perform numerical modeling for reproducing experimentally observed features not only qualitatively but also quantitatively.

ACKNOWLEDGMENT

We acknowledge support from DFG SPP 1839 and the MWK Baden-Württemberg.

[1] G. Agrawal, *Nonlinear Fiber Optics* (Academic Press, San Diego, 2001).
[2] R. Carman, R. Chiao, and P. Kelley, Phys. Rev. Lett. **17**, 1281 (1966).
[3] R. Stolen, J. Bjorkholm, and A. Ashkin, Appl. Phys. Lett. **24**, 308 (1974).
[4] C. Lin, W. A. Reed, A. D. Pearson, and H.-T. Shang, Opt. Lett. **6**, 493 (1981).
[5] K. Hill, D. Johnson, B. Kawasaki, and R. MacDonald, J. Appl. Phys. **49**, 5098 (1978).
[6] R. Stolen and J. Bjorkholm, IEEE J. Quantum Electron. **18**, 1062 (1982).
[7] P. Baldeck and R. Alfano, J. Lightwave Technol. **5**, 1712 (1987).
[8] K. Washio, K. Inoue, and S. Kishida, Electron. Lett. **16**, 658 (1980).
[9] M. Marhic, N. Kagi, T.-K. Chiang, and L. Kazovsky, Opt. Lett. **21**, 573 (1996).
[10] I. Malitson, J. Opt. Soc. Am. **55**, 1205 (1965).
[11] A. Börzsönyi, Z. Heiner, M. Kalashnikov, A. Kovács, and K. Osvay, Appl. Opt. **47**, 4856 (2008).
[12] F. Benabid and P. Roberts, J. Mod. Opt. **58**, 87 (2011).
[13] P. St. J. Russell, P. Hölzer, W. Chang, A. Abdolvand, and J. Travers, Nat. Photonics **8**, 278 (2014).
[14] R. Sollapur, D. Kartashov, M. Zürch, A. Hoffmann, T. Grigorova, G. Sauer, A. Hartung, A. Schwuchow, J. Bierlich, J. Kobelke *et al.*, Light Sci. Appl. **6**, e17124 (2017).
[15] M. Nisoli, S. Stagira, S. De Silvestri, O. Svelto, S. Sartania, Z. Cheng, M. Lenzner, C. Spielmann, and F. Krausz, Appl. Phys. B **65**, 189 (1997).
[16] S. Hädrich, H. Carstens, J. Rothhardt, J. Limpert, and A. Tünnermann, Opt. Express **19**, 7546 (2011).
[17] C. R. Rosberg, F. H. Bennet, D. N. Neshev, P. D. Rasmussen, O. Bang, W. Krolikowski, A. Bjarklev, and Y. S. Kivshar, Opt. Express **15**, 12145 (2007).
[18] J. Bethge, A. Husakou, F. Mitschke, F. Noack, U. Griebner, G. Steinmeyer, and J. Herrmann, Opt. Express **18**, 6230 (2010).
[19] M. Vieweg, T. Gissibl, S. Pricking, B. Kuhlmey, D. Wu, B. Eggleton, and H. Giessen, Opt. Express **18**, 25232 (2010).
[20] M. Chemnitz, M. Gebhardt, C. Gaida, F. Stutzki, J. Kobelke, J. Limpert, A. Tünnermann, and M. A. Schmidt, Nat. Commun. **8**, 42 (2017).
[21] M. Zeisberger, A. Hartung, and M. A. Schmidt, Fibers **6**, 68 (2018).
[22] A. Snyder and J. Love, *Optical Waveguide Theory* (Chapman and Hall, London, 1983).
[23] R. Sammut and A. Snyder, Appl. Opt. **15**, 477 (1976).
[24] R. Sammut and A. Snyder, Appl. Opt. **15**, 1040 (1976).
[25] C. Sauvan, J. P. Hugonin, I. S. Maksymov, and P. Lalanne, Phys. Rev. Lett. **110**, 237401 (2013).
[26] S. Upendar, I. Allayarov, M. A. Schmidt, and T. Weiss, Opt. Express **26**, 22536 (2018).
[27] E. Muljarov, W. Langbein, and R. Zimmermann, Europhys. Lett. **92**, 50010 (2011).
[28] M. B. Doost, W. Langbein, and E. A. Muljarov, Phys. Rev. A **87**, 043827 (2013).
[29] T. Weiss, M. Schäferling, H. Giessen, N. A. Gippius, S. G. Tikhodeev, W. Langbein, and E. A. Muljarov, Phys. Rev. B **96**, 045129 (2017).
[30] E. Muljarov and T. Weiss, Opt. Lett. **43**, 1978 (2018).
[31] I. Allayarov, S. Upendar, M. A. Schmidt, and T. Weiss, Phys. Rev. Lett. **121**, 213905 (2018).
[32] A. Maslov, Opt. Lett. **39**, 4396 (2014).
[33] G. Li, C. M. de Sterke, and S. Palomba, Opt. Lett. **42**, 1329 (2017).
[34] M. M. Elsawy and G. Renversez, Opt. Lett. **43**, 2446 (2018).
[35] S. Afshar and T. M. Monro, Opt. Express **17**, 2298 (2009).
[36] R. W. Boyd, *Nonlinear Optics* (Academic Press, New York, 2003).
[37] C. Sauteret, J.-P. Hermann, R. Frey, F. Pradere, J. Ducuing, R. H. Baughman, and R. Chance, Phys. Rev. Lett. **36**, 956 (1976).

[38] L. Acioli, A. Gomes, and J. R. Leite, Appl. Phys. Lett. **53**, 1788 (1988).
[39] B. Lawrence, W. E. Torruellas, M. Cha, M. L. Sundheimer, G. I. Stegeman, J. Meth, S. Etemad, and G. Baker, Phys. Rev. Lett. **73**, 597 (1994).
[40] R. Stolen, J. P. Gordon, W. J. Tomlinson, and H. A. Haus, J. Opt. Soc. Am. B **6**, 1159 (1989).
[41] B. D. Guenther and D. Steel, *Encyclopedia of Modern Optics*, (Academic Press, New York, 2018), Vol. 4.
[42] A. M. Zheltikov, Opt. Lett. **32**, 2052 (2007).
[43] E. E. Serebryannikov and A. M. Zheltikov, Phys. Rev. A **76**, 013820 (2007).
[44] R. L. Sutherland, *Handbook of Nonlinear Optics* (Marcel Dekker, New York, 2003).
[45] W. van Saarloos and P. Hohenberg, Physica D **56**, 303 (1992).
[46] I. M. Allayarov and E. N. Tsoy, Phys. Lett. A **377**, 550 (2013).
[47] V. Vasiliev, Y. M. Romanovskii, D. Chernavskii, and V. Yakhno, *Autowave Processes in Kinetic Systems: Spatial and Temporal Self-Organisation in Physics, Chemistry, Biology, and Medicine* (Springer, New York, 1987).
[48] P. Grelu and N. Akhmediev, Nat. Photon. **6**, 84 (2012).
[49] T. J. Bridges and F. Dias, Phys. Fluids **19**, 104104 (2007).
[50] E. A. Golovchenko and A. N. Pilipetskii, J. Opt. Soc. Am. B **11**, 92 (1994).
[51] H. Garcia, A. M. Johnson, F. A. Oguama, and S. Trivedi, Opt. Lett. **28**, 1796 (2003).
[52] A. Börzsönyi, Z. Heiner, M. Kalashnikov, A. Kovács, and K. Osvay, Opt. Express **18**, 25847 (2010).
[53] D. Marcuse, *Light Transmission Optics* (Van Nostrand Reinhold, New York, 1972).
[54] N. Litchinitser, A. Abeeluck, C. Headley, and B. Eggleton, Opt. Lett. **27**, 1592 (2002).
[55] See Supplemental Material at http://link.aps.org/supplemental/10.1103/PhysRevA.101.043806 for additional details as well as the complete dispersion, loss, and nonlinearity parameters of our simulations.
[56] K. Blow and D. Wood, IEEE J. Quantum Electron. **25**, 2665 (1989).
[57] I. Cristiani, R. Tediosi, L. Tartara, and V. Degiorgio, Opt. Express **12**, 124 (2004).